

Magnetic Field Variations Near Weak Magnetic Materials Studied by Magnetic Resonance Imaging Techniques

I. Frollo¹, P. Andris¹, D. Gogola¹, J. Přebil¹, L. Valkovič^{1,2}, and P. Szomolányi^{1,2}

¹Institute of Measurement Science, Slovak Academy of Sciences, 841 04 Bratislava, Slovakia

²MR Centre-Highfield MR, Department of Radiology, Medical University of Vienna/Vienna General Hospital, A-1090 Vienna, Austria

Imaging based on magnetic resonance (MRI) for mapping and imaging of the weak magnetic materials placed into the homogenous magnetic field of an imager is proposed. Samples made of weak magnetic material were theoretically computed, constructed, and tested on an MRI 0.178 T permanent magnet imager. In laboratory experiments, a homogeneous phantom (reference medium)—a container filled with doped water—was used. The resultant image represents the magnetic field variations (MFV) in the homogeneous phantom. For detection, a carefully tailored gradient-echo (GRE) imaging method, susceptible to magnetic field homogeneities, was used. The first results showed the feasibility of the method and some of the possibilities offered in this field for material research.

Index Terms—Gradient echo, magnetic resonance imaging, soft magnetic materials.

I. INTRODUCTION

WEAK magnetic materials are widely used for electric and electronic devices. Weak magnetic materials belong to diamagnetic and paramagnetic materials. Values of susceptibility defined as $\chi_i = (dM/dH)_0$, i.e., change in magnetization with the change in field at the origin (M —magnetization, H —magnetic field, whereas $M = \chi H$), range from around -10^{-5} in very weak magnetic materials up to values of around $+10^6$ in ultra-soft ferromagnets, [1].

Imaging of proton density based on magnetic resonance (MR) methods used for biological and physical structures is a routine investigating procedure. Special case is observed when an object that consists of a weak magnetic material is inserted into a stationary homogeneous magnetic field. This results in a variation of the basic stationary magnetic field. Using a dedicated homogeneous phantom filled with doped water near the sample enabled to image the contours of this sample. The acquired image represents a modulation of the basic magnetic field of the imager detectable by gradient echo imaging sequence.

First attempts of a direct measurement of the magnetic field created in living and physical tissue by a simple wire fed by a current were reported in [2]. The motion of magnetization during applications of electric current and radio-frequency (RF) pulses was formulated based on the rotating frame Bloch equation. Images of a phantom were obtained with and without application of the electric current to a straight wire. Sensitivity of MR imaging to magnetic field variations using small electric currents flowing in the human body was studied in [3]. The influence of a susceptibility artifact on the detection threshold and sensitivity was shown in [4]. For this purpose a novel phantom, consisting of a water-filled cylinder with two wires of different material connected in series, was constructed.

The prospective advantage of MRI is limited by artifacts due to the presence of metallic materials. An example related to the quantitative evaluation of the magnitude of artifacts from dental casting alloys and implant materials in MRI, dental casting or implant materials imaged by means of 1.5 T MRI apparatus was described in [5].

Magnetic susceptibility of materials that are used for body implants causes much distortion in MR images; this was shown in [6]. A modified spin-echo method, in which inserting a time interval of a defined length reduced the range of phase modulation below the value of 2π , was used. Several experiments with indirect susceptibility mapping of thin-layer samples using MR imaging of a planar paramagnetic sample and a homogeneous phantom were reported in [7]. Reduction of artifacts of metallic implant in MRI by coating of diamagnetic material was discussed in [8]. Two models investigating the effect of susceptibility of the paramagnetic and diamagnetic materials are shown. Susceptibility artifacts appeared with the presence of metal from biopsy conventional titanium tissue marker clips [9]. This study compared the size of MR susceptibility artifacts and the degree of local spectroscopy signal disturbance. The basic concept of magnetic susceptibility as an important field in MRI with medical orientation was reported in [10]. The magnetic susceptibility effects influence the development of MR guided surgery, construction of surgical instruments and other devices with susceptibility tailored to the MR environment.

Susceptibility effects of iron-containing brain structures were qualitatively analyzed by comparing the degree of visible hypointensity by a score system at either field strength, [11]. The paper presents phantom experiments, where T_2 -weighted fast spin-echo images at 1.5 T and 3.0 T of iron oxide phantoms with different iron oxide concentration Fe/ml saline were measured and compared. The susceptibility aspects of contrast agents for MRI and molecular imaging are significant in the field of biomedical nanomagnetism [12]. The intensity of the MRI signal from a tissue is a function of the density of protons, the relaxation times, the magnetic susceptibility and any motion of the tissue.

A computer simulation program capable of demonstrating various artifacts, such as image distortion caused by metallic implants in MR imaging, was presented in [13]. The structure

Manuscript received September 14, 2011; revised January 16, 2012; accepted March 08, 2012. Date of publication March 19, 2012; date of current version July 20, 2012. Corresponding author: I. Frollo (e-mail: frollo@savba.sk).

Color versions of one or more of the figures in this paper are available online at <http://ieeexplore.ieee.org>.

Digital Object Identifier 10.1109/TMAG.2012.2191298

of the program allows various imaging situations respecting the Bloch equations.

Numerical modeling of magnetic field variations in the environment of measured diamagnetic and paramagnetic samples, for the purposes of studying MR image variations owing to the susceptibility of heterogeneous materials, was described in [14]. The verification was carried out using a simple sample configuration (circular plate), and the numerically modeled cross sections were compared with the values of the magnetic field, experimentally measured by the MR gradient echo technique. Magnetic susceptibility measurement using MR tomography with analytical calculation was presented in [15].

The magnetic field properties of body tissue and contrast agents, along with the influence of magnetic susceptibility effects on imaging were discussed in [16].

In this paper we explore possibilities of detection of selected weak magnetic materials using an imaging method based on MR principles.

The goal of this paper was to provide a theoretical analysis and experimental measurements of magnetic field variations of rectangular and circular magnetic double layers. Theoretical calculations and simulations demonstrate the potential and expectations from images measured by a low-field MRI instrument. Our experimental task was to map the magnetic field variation and to image the specific structure of thin ferromagnetic or paramagnetic samples using a special plastic holder. Carefully tailored gradient echo MRI measuring sequences were used. A series of selected images of thin objects shows the perspective possibilities of application of this methodology.

II. THEORETICAL ANALYSIS

Let us assume an ideally homogeneous magnetic field of an MR imager. When a ferromagnetic or paramagnetic object is placed into this homogeneous magnetic field, the field near the sample is distorted.

For the theoretical analysis and optimal physical interpretation, a magnetic double layer model is used [17].

A. Rectangular Sample

For the purpose of our simple example we suppose that the magnetic double layer is positioned in the x-y plane of the rectangular coordinate system ($\mathbf{i}_x, \mathbf{j}_y, \mathbf{k}_z$) and the thickness of the layer is neglected.

According to Fig. 1, we suppose the layer is limited by lengths of $2a$ and b , with the left—right symmetry. The layer is moved in $+y$ direction by distance g , $ds[x,y]$ is an elementary surface element. The basic magnetic field B_0 of the MR imager is parallel with the z-axis. The task is to calculate the $B_z(x, y, z)$ component of the magnetic field in point $A[x_0, y_0, z_0]$.

In a general definition, the magnetic layer with magnetic dipoles continuously distributed on surface S can be considered. Such planar magnetic dipole distribution is called magnetic

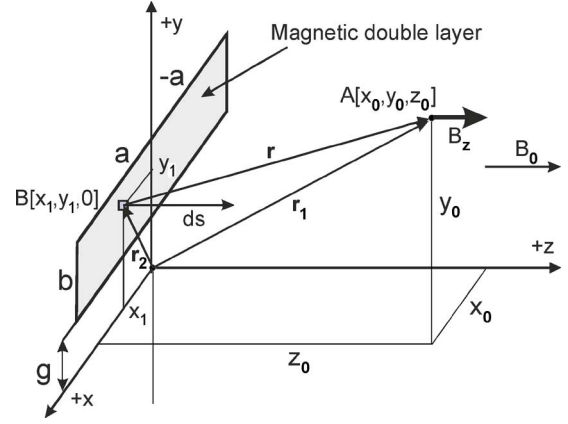


Fig. 1. Basic configuration of the magnetic double layer rectangular sample positioned in x-y plane of the rectangular coordinate system. The thickness of the layer is neglected.

double layer and is characterized by the surface density of a magnetic dipole moment \mathbf{M} :

$$\mathbf{m}_s = \int_S \mathbf{M}_S(\mathbf{r}) dS \quad \text{and} \quad \mathbf{M}_S = I \mathbf{n} \quad (1)$$

where

- \mathbf{m}_s magnetic dipole moment in a particular point;
- \mathbf{r} position vector;
- I current equivalent to planar density of dipole moment of the magnetic double layer;
- \mathbf{n} unit normal vector of surface S in a particular point.

The formula for magnetic field in point $A[x_0, y_0, z_0]$ requires the use of the Biot-Savart law [18] in vector form, assuming the known equivalency of a current loop and a magnetic double layer (the curve integral is replaced by a surface integral):

$$\mathbf{B} = -\frac{\mu_0 I}{4\pi} \oint \frac{\mathbf{r} \times d\mathbf{l}}{r^3} = \frac{\mu_0 I}{4\pi} \int_S \left(\frac{3\mathbf{r} \cdot \mathbf{r}}{r^5} - \frac{\mathbf{I}}{r^3} \right) ds. \quad (2)$$

From the physical interpretation assuming:

$$\mathbf{r} \cdot \mathbf{r} = r^2 = (x_0 - x)^2 + (y_0 - y)^2 + (z_0 - z)^2 \quad (3)$$

we can write the final formula for the magnetic field in a double integral form as follows:

$$B_z(x, y, z) = \frac{\mu_0 I}{4\pi} \int_{-a}^a \left[\int_d^h \frac{3 - I}{r^3} dy \right] dx \quad (4)$$

where limits for integration are: $[-a, a]$ and $[d = g, h = g + b]$, see Fig. 1.

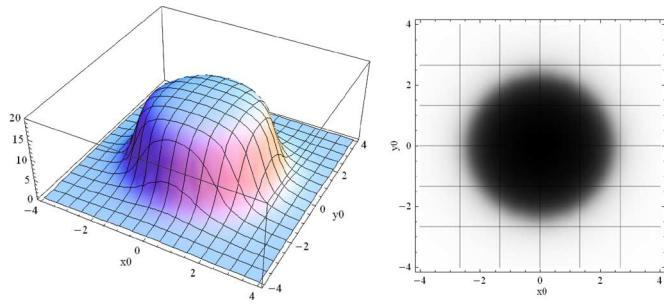


Fig. 5. Calculated magnetic field $B_z(x, y, z)$ of the magnetic double layer of the circular sample in the x - y plane for incremental calculation. Left: 3-D plot. Right: density plot.

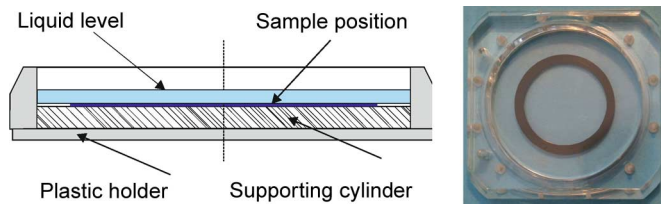


Fig. 6. Left: Plastic holder used for sample positioning. Right: Dish for the testing liquid. Circular sample dimensions: $D_1 = 60$ mm, $D_2 = 50$ mm.

The half length of the strip is $t_n = \sqrt{R^2 - a_n^2}$, the width of the strip is d . The final formula, using expression (4), represents the sum of partial element contributions of the upper and lower part of the disc:

$$B_z(x, y, z) = \frac{\mu_0 I (3 - I)}{4\pi} \sum_{-n}^n \left(\int_{a_n - d}^{a_n} \left[\int_{-t_n}^{t_n} \frac{1}{r^3} dx \right] dy \right) + \frac{\mu_0 I (3 - I)}{4\pi} \sum_{-n}^n \left(\int_{-a_n}^{-a_n + d} \left[\int_{-t_n}^{t_n} \frac{1}{r^3} dx \right] dy \right). \quad (8)$$

Assuming the following relative values: $\mu_0 I (3 - I) / 4\pi = 1$, $R = 3$, $d = 0.1R$, $z_0 = 0.1R$, $z_0 = 0.5$, the resultant 3-D and density plots of the magnetic field of the relative values for $\{x_0, -4, 4\}$, $\{y_0, -4, 4\}$ are depicted in Fig. 5.

III. EXPERIMENTAL SETUP

For the purpose of our experiments an MR imager, permanent magnet 0.178 T (Esaote, Genoa, Italy) with vertical orientation of the basic magnetic field B_0 , was used.

A circular plastic holder used for sample positioning and a dish for testing liquid is depicted in Fig. 6. A flat supporting cylinder made of Plexiglas was placed at the bottom of the plastic holder. A very thin isolating membrane was placed on its upper part, separating the sample from the liquid. The height of liquid could be up to 15 mm. The liquid contained 5 mM $\text{NiCl}_2 + 55$ mM NaCl in distilled water. This solution was used to shorten the repetition time TR of the imaging sequence GRE due to its reduction of H_2O relaxation T_1 (to speed up the data collection).



Fig. 7. Horizontal field hand/wrist RF coil and plastic holder (homogeneous phantom), active circular diameter 90 mm.

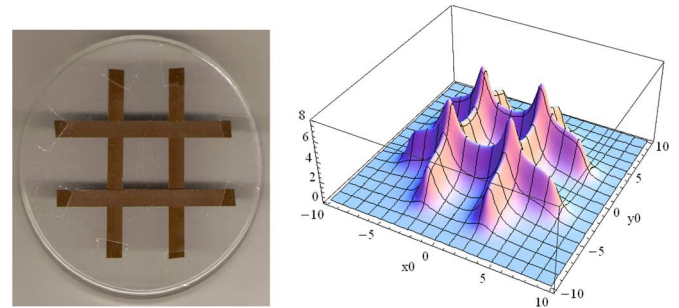


Fig. 8. Left: Original sample made of 4 low magnetic tapes, “double cross,” 6 mm \times 70 mm, distance between tapes 25 mm, audio cassette tape, thickness 11 μm , densely packed pure grained ferric particles. Right: Calculated 3-D image of the magnetic field distribution for $z_0 = 0.5$.

The general configuration of an RF coil and the plastic holder is shown in Fig. 7.

An RF hand/wrist transducing coil (elliptical solenoid) together with the phantom was placed into the center of the permanent magnet, perpendicular to the magnetic field (B_0) orientation.

The GRE MR sequences were selected for the measurements [17], [20]. A special feature of this sequence is its sensitivity to basic magnetic field inhomogeneities. The actual parameters used in the presented experiments are as follows: RF pulse: 90° , repetition time: TR = 800 ms, echo time: TE = 10 ms, number of averages: 6, measured matrix: 256×256 , field of view: 140×140 , imaged thickness: 2.0–3.0 mm.

IV. EXPERIMENTAL IMAGING AND RESULTS

As the first physical model, a sample made of four standard low magnetic tapes was used. The sample was placed into the center of a plastic holder—homogeneous phantom filled with the above mentioned solution, see Fig. 6.

3-D plot and density plot images of the magnetic field distribution were calculated using formula (5) respecting the dimensions and positions of particular parts of the samples, see Figs. 8 and 9.

In the second experimental example—circular model, annulus—a sample was cut from low magnetic floppy disk. The sample was placed into the center of a plastic holder, see Fig. 6. 3-D plot and density plot images of the magnetic field distribution were calculated using formula (8) respecting the dimensions and positions of the particular strips. Two disks were calculated, relative values $R_1 = 3.0$ and $R_2 = 2.5$, $d_1 = 0.1R_1$, $d_2 = 0.1R_2$, $z_0 = 0.1R_1$. The smaller disc

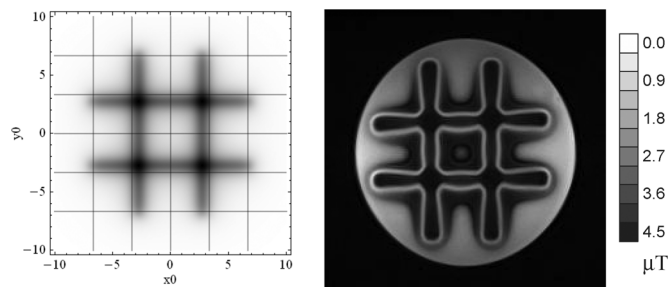


Fig. 9. Left: Calculated image of the magnetic field, density plot, $z_0 = 0.5$. Right: MR image of the double cross sample using the GRE imaging sequence.

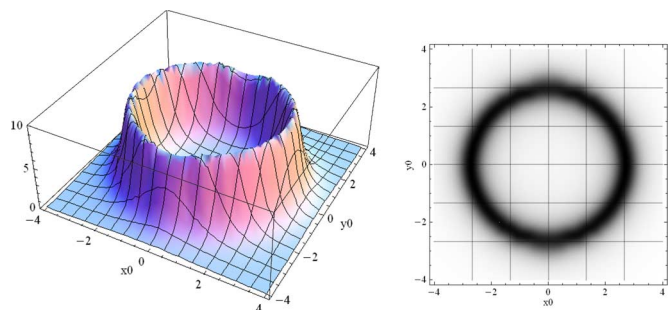


Fig. 10. Calculated magnetic field of the magnetic annulus. Left: 3-D image. Right: density plot.

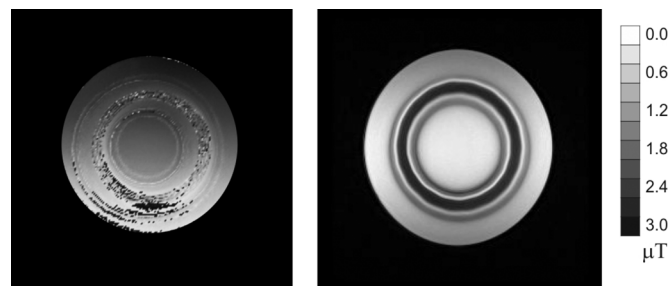


Fig. 11. Left: Phase image calculated from the measured data. Right: Magnitude image of the magnetic annulus. Number of measured samples, measured matrix: 256×256 . Actual image of this sample was associated with 125×125 pixels.

data was subtracted from the bigger disk data. Resultant magnetic field of the calculated annulus of the relative values for $\{x_0, -4, 4\}$, $\{y_0, -4, 4\}$ is in Fig. 10.

The MR image of the magnetic annulus and the calculated phase image from the measured data are depicted in Fig. 11. The MR image representing magnetic field variation and the phase image were calculated from measured data using a classic GRE sequence. The measurement was performed two times with different echo times TE. The Fourier transformed data matrices were ratio processed to prevent phase wrapping and to remove some distortions [19]. The magnetic field scale relates to the circular image of the sample. The noise in the phase image is caused by limited phase unwrapping due to a very long time interval between both echo times, set as default by the used MR scanner.

Several imaging experiments were carried out on very silky samples, textile material treated by magnetic nanoparticles, biological samples, documents equipped with hidden magnetic do-



Fig. 12. MR image of the polymer fiber, thickness 0.14 mm, treated by the water solution of Fe_3O_4 nanoparticles. Number of measured samples, measured matrix: 256×256 . Actual image of this sample was associated with 100×100 pixels.

main, banknotes, etc. One example, a polymer fiber treated by the water solution of Fe_3O_4 nanoparticles, is given in Fig. 12.

V. CONCLUSION

The goal of this study was to mathematically describe and experimentally measure the MFV caused by weak magnetic materials using an imaging method based on MR principles. Mathematical analysis of rectangular and circular objects, representing a shaped magnetic double layer, showed theoretical possibilities to calculate magnetic field around any type of sample. Calculated 3-D images showed expected shapes of the magnetic field in the vicinity of the double layer samples. Density plot images showed magnetic field variations caused by samples placed into the homogeneous magnetic field of the MR tomograph. Our experiments proved that it is possible to map the magnetic field variations and to image the specific structures of thin ferromagnetic or paramagnetic samples using a special plastic holder. Carefully designed GRE measuring sequences were used. The shapes of experimental MR images, Fig. 9, 11 and 12, correspond to the real shapes of the samples. The resultant MR images are encircled by narrow stripes that optically extend the width of the sample. This phenomenon is typical for susceptibility imaging, when one needs to measure local magnetic field variations representing sample properties [15], [16]. In the presented calculations, the bright edges phenomena seen in the images are not considered due to their very high mathematical complexity. It is a limitation of the current study and will be solved in our future work.

It is evident that imaging of the magnetic field variations of the weak magnetic samples can be performed by the GRE method based on the transfer of magnetic properties of the sample into the homogeneous planar phantom. This effect is strongest if the vector of the static magnetic field $B_0 = B_z$ is perpendicular to the sample plain. Our experimental results are in good correlation with the mathematical simulations. This validates the possible suitability of the proposed method for detection of weak magnetic materials using the MRI methods. Presented images of thin objects indicate perspective possibilities of this methodology even in the low-field MRI.

ACKNOWLEDGMENT

This work was supported by the Slovak Scientific Grant Agency VEGA 2/0090/11, State program SPVV no. 2003SP200280203 and by the project CEKOMAT, ITMS No. 26240120006 based on the support of Operational Program Research and Development, financially supported by the European Regional Development Fund.

REFERENCES

- [1] É. Du Trémolet de Lacheisserie, D. Gignoux, and M. Schlenker, *Magnetism: Fundamentals*: First Springer Science+Business Media, Inc., 2005, 0-387-23062-9, softcover printing, E-book.
- [2] M. Sekino, T. Matsumoto, K. Yamaguchi, N. Iriguchi, and S. Ueno, "A method for NMR imaging of a magnetic field generated by electric current," *IEEE Trans. Magn.*, vol. 40, no. 4, pp. 2188–2190, Jul. 2004.
- [3] M. Joy, G. Scott, and M. Henkelman, "In vivo imaging of applied electric currents by magnetic resonance imaging," *Magn. Reson. Imag.*, vol. 7, pp. 89–94, 1989.
- [4] R. Huang, O. Posnansky, A. Celik, A.-M. Oros-Peusquens, V. Ermer, M. Irkens, and N. J. Shah, "Measurement of weak electric currents in copper wire phantoms using MRI: Influence of susceptibility enhancement," *Magn. Reson. Mater. Phys., Biol. Med.*, vol. 19, pp. 124–133, 2006.
- [5] F. Shafiei, E. Honda, H. Takahashi, and T. Sasaki, "Artifacts from dental casting alloys in magnetic resonance imaging," *J. Dental Res.*, vol. 82, no. 8, pp. 602–606, 2003.
- [6] K. Bartusek, Z. Dokoupil, and E. Gescheidtova, "Magnetic field mapping around metal implants using an asymmetric spin-echo MRI sequence," *Meas. Sci. Technol.*, vol. 17, no. 12, pp. 3293–3300, 2006.
- [7] I. Frollo, P. Andris, J. Přibil, and V. Juráš, "Indirect susceptibility mapping of thin-layer samples using nuclear magnetic resonance imaging," *IEEE Trans. Magn.*, vol. 43, no. 8, pp. 3363–3367, Aug. 2007.
- [8] Y. Gao, K. Muramatsu, A. Kushibe, K. Yamazaki, A. Chiba, and T. Yamamoto, "Reduction of artifact of metallic implant in magnetic resonance imaging by coating of diamagnetic material," *IEEE Trans. Magn.*, vol. 45, no. 10, pp. 4837–4840, Oct. 2009.
- [9] S. V. Ghate, J. A. Baker, A. D. Hawkins, and B. J. Soher, "Titanium vs carbon coated ceramic breast tissue marker clips: 3T MR susceptibility artifact and local signal disturbance," *Acad. Radiol.*, vol. 18, no. 6, pp. 770–773, Jun. 2011.
- [10] J. F. Schenck, "The role of magnetic susceptibility in magnetic resonance imaging: MRI magnetic compatibility of the first and second kinds," *Med. Phys.*, vol. 23, no. 6, pp. 815–850, 1996.
- [11] T. Allkemper, W. Schwandt, D. Maintz, W. Heindel, and B. Tombach, "Sensitivity of T2-weighted FSE sequences towards physiological iron depositions in normal brains at 1.5 and 3.0 T," *Eur. Radiol.*, vol. 14, no. 6, pp. 1000–1004, 2004.
- [12] K. M. Krishnan, "Biomedical nanomagnetics: A spin through possibilities in imaging, diagnostics, and therapy," *IEEE Trans. Magn.*, vol. 46, no. 7, pp. 2523–2558, Jul. 2010.
- [13] M. B. E. Olsson, R. Wirestam, and B. R. R. Persson, "A computer simulation program for MR imaging: Application to RF and static magnetic field imperfections," *Magn. Reson. Med.*, vol. 34, no. 4, pp. 612–617, 1995.
- [14] K. Bartusek, P. Fiala, and J. Mikulka, "Numerical modeling of magnetic field deformation as related to susceptibility measured with an MR system," *Radioengineering*, vol. 17, no. 4, pp. 113–118, 2008.
- [15] M. Steinbauer and K. Bartušek, "Magnetic susceptibility measurement using magnetic resonance tomography," *Acta Technica ČSAV*, vol. 53, no. 1, pp. 45–63, 2008.
- [16] E. M. Haacke, R. W. Brown, M. R. Thompson, and R. Venkatesan, *Magnetic Resonance Imaging: Physical Principles and Sequence Design*, 1st ed. New York: Wiley-Liss, John Wiley and Sons, 1999.
- [17] C. Mueller, G. Scheinert, and F. H. Uhlmann, "Sensitivity estimation for magnetic devices using a double-layer model," in *International Journal of Applied Electromagnetics and Mechanics*. Amsterdam, The Netherlands: IOS Press, 2003, vol. 17, pp. 221–230.
- [18] J. D. Kraus and D. A. Fleisch, *Electromagnetics With Applications*, 5th ed. New York: McGraw-Hill Series in Electrical & Computer Engineering, 1999, 0-07-289969-7.
- [19] P. Andris and I. Frollo, "Optimized measurement of magnetic field maps using nuclear magnetic resonance (NMR)," *Meas. Sci. Technol.*, vol. 22, no. 4, pp. 1–8, 2011, 045501.
- [20] J. Jianming, *Electromagnetic Analysis and Design in Magnetic Resonance Imaging*, ser. Biomedical Engineering Series, M. R. Neuman, Ed. Boca Raton, FL: CRC Press, 1999.